Predictive Dynamic Model of Single-Stage Ultra-Rapid Pressure Swing Adsorption

E. M. Kopaygorodsky, V. V. Guliants, and W. B. Krantz
Dept. of Chemical and Materials Engineering, University of Cincinnati, Cincinnati, OH 45221

DOI 10.1002/aic.10093
Published online in Wiley InterScience (www.interscience.wiley.com).

A dynamic model is developed based on the preliminary set of assumptions to determine the viability of a pulsed Ultra-Rapid Pressure Swing Adsorption (URPSA) air-separation process using a 5A zeolite monolith adsorbent. The new model was shown to predict the performance of the Rapid PSA process investigated experimentally in 1986 by Pritchard and Simpson. The model predicts that single-stage URPSA is capable of producing oxygen purities of 85%, product recoveries of around 60%, and a bed-size factor of around 0.00073. A very small bed-size factor and large product recoveries are characteristic of this novel process, which implies improved efficiency of separation per unit mass of adsorbent material. The model developed here provides the first assessment of the viability of ultra-rapid cycles and thin monolithic adsorbents for air separation by PSA. © 2004 American Institute of Chemical Engineers *AIChE J,* 50: 953–962, 2004
Keywords: pressure swing adsorption, ultra-rapid, air separation, zeolite, model

Introduction

Conventional PSA is responsible for 20% of the world's oxygen production. The conventional PSA process is shown in Figure 1. The conventional PSA process consists of two adsorption beds, packed with adsorbent material, and operates on a Skarstrom cycle. The basic Skarstrom PSA cycle involves four distinct steps. During step 1, a high-pressure feed is supplied continuously to bed 2 in which preferential adsorption of the more strongly adsorbed component occurs. The less strongly adsorbed component is collected as a product. In step 2, bed 1 is pressurized with feed, whereas bed 2 is blown down in the reverse flow direction. The same cycle is repeated in steps 3 and 4 with bed 1 being pressurized and bed 2 purged. The Skarstrom cycle ensures continuous product collection. Modeling of the conventional two-bed process started in the early 1960s. Carter (1966) and other pioneers of PSA modeling assumed the bulk gas is in instantaneous equilibrium with the adsorbent during all four steps in the cycle. Shendalman and Mitchell (1972) were the first to replace the gas/adsorbent equilibrium assumption by a linear driving force approximation, suggested by Glueckauf and Coates (1947). This linear driving force approximation took into consideration mass-transfer limitations in the pores of the adsorption bed. Since then, a multitude of mathematical models for conventional PSA have been developed [Farooq et al. (1989); Hassan and Ruthven (1986); Liow and Kenney (1990); Mendes and Costa (1999); Raghavan et al. (1985); Shin and Knaebel (1987); Singh and Jones (1987); Teague and Edgar (1999)]. They differ in the type of assumptions made: isothermal or nonisothermal process, the presence or absence of axial dispersion, assumptions regarding rate limiting or equilibrium adsorption rate, whether the pressure drop ascribed to viscous forces is accounted for, and the nature of the boundary and initial conditions. The interested reader is referred to the comprehensive review of conventional PSA modeling by Ruthven et al. (1994).

The conventional PSA process suffers from low separation efficiency per unit mass of adsorbent material, large capital investments for replacement of adsorbent material attributed to the particle attrition, and complexity of the piping network. Current trends in PSA research involve addressing these limitations of conventional PSA by investigating the concept of a pulsed PSA process. Development of the conventional two-bed

Correspondence concerning this article should be addressed to V. V. Guliants at vguliant@alpha.che.uc.edu.

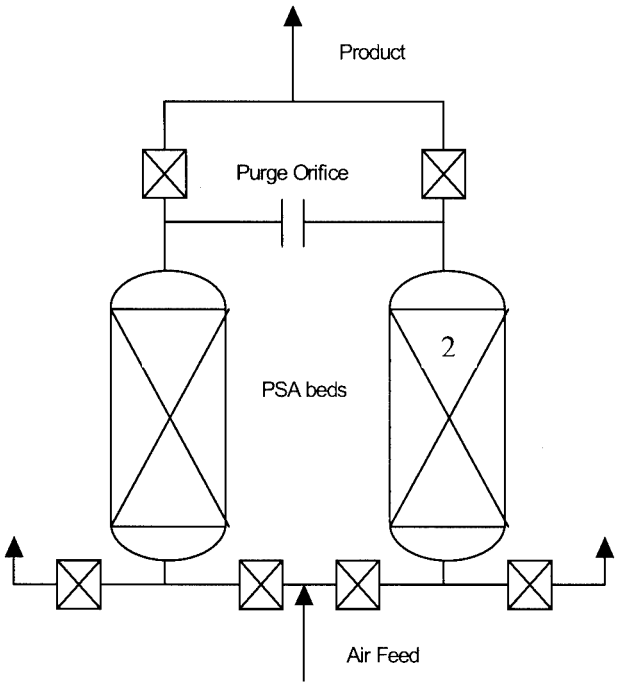

Figure 1. Conventional two-bed PSA process.

PSA process is directed toward improving the separation efficiency per unit mass of adsorbent material by reducing the size of the adsorbent particles, reducing the complexity of the piping network by using a single adsorption bed, and reducing the impact of the pressure drop by making the adsorption bed shorter than that of conventional design. Figure 2 shows a pulsed PSA. The operation cycle of the pulsed PSA process involves four steps: pressurization, delay, depressurization, and purge. The first published account of a pulsed PSA process was by Turnock and Kadlec (1971). Jones and Keller (1981) patented the Rapid PSA (RPSA) process in 1980. These two researchers found that a short bed, filled with small adsorbent particles (20–120 mesh), allows for faster cycling and substantially higher product recovery. Their intensified PSA process improved oxygen productivity per unit mass of adsorbent five times when compared to a conventional two-bed PSA process. Jones and Keller also proposed short pressurization times (t_{pres} $<$ 1.0 s) and long depressurization times (t_{depres} = 5–20 s). With the publication of a patent by Jones and Keller in 1980 came a new wave of modeling studies. These include the following publications: Alpay et al. (1993); Hart and Thomas (1991); Pritchard and Simpson (1986); and Rota and Wankat (1990). These models relax most of the assumptions made in conventional analyses including negligible pressure drop in the bed and insignificant axial dispersion. The combination of rapid cycling and small particles leads to steep and cyclically varying pressure gradients within the bed, which dictates the use of the Ergun equation to account for viscous drag in the bed. Alpay et al. (1993) developed a comprehensive theoretical model of the pulsed RPSA process. Their work concluded that the separation capabilities of the pulsed RPSA cycle are the best for adsorption beds packed with 250- to 350-micron particles.

For reasons similar to those for the conventional two-bed PSA process, pulsed PSA suffers from low efficiency of separation per unit mass of adsorbent material, particle attrition, and low throughputs arising from a larger pressure drop in the packed bed of smaller particles. Ultra-Rapid PSA is investigated here as a possible solution to the limitations of conventional and pulsed pressure swing adsorption. The potential of this process for air separation has not been investigated before.

URPSA is shown in Figure 3. URPSA involves using a thin bed (2 mm) of monolithic adsorbent (5A zeolite) and ultra-rapid PSA cycles that consist of two steps: pressurization and depressurization ($<$3 s). During a typical pressurization step in the cycle for air separation, an absolute pressure of 150 kPa is applied to the surface of the adsorbent bed for 1 s. Because the product side of the bed is at atmospheric pressure, a pressure gradient is created and air flows through the adsorbent. The more strongly adsorbed component is retained in the bed and oxygen-enriched gas is collected as a product. During the depressurization step of the cycle, the feed surface of the adsorbent is typically exposed to atmospheric pressure for 2 s, which ensures bed regeneration. The purpose of this article is to develop a mathematical model for this process. Once the model is developed, this article will show the effectiveness of scaling analysis in justifying the assumptions frequently made by others based on pure intuition. Then, the scaled and simplified model is used to assess the viability of URPSA as more efficient technique for air separation by determining the following model performance characteristics: oxygen purity, product recovery, and bed-size factor. In addition, this article will show the impact of feed pressure, pressurization time, and depressurization time on predicted performance characteristics.

Theoretical Model

To develop a mathematical model for this process the following assumptions are introduced:

(1) The system is assumed to be isothermal. In conventional large-scale systems this would be a tenuous assumption. However, in this study the small adsorption bed and the high heat capacity of the material that surrounds it minimize the temperature fluctuations.

(2) Darcy's law describes the gas flow. In conventional PSA the frictional pressure drop in the bed is often assumed to be negligible without any justification. However, in this research, the pressure drop attributed to the viscous drag is important because of the mesoporosity of the adsorption bed.

(3) The monolithic 5A zeolite adsorbent bed is assumed to have uniform voidage, zeolite particle size, and spherical zeolite particles.

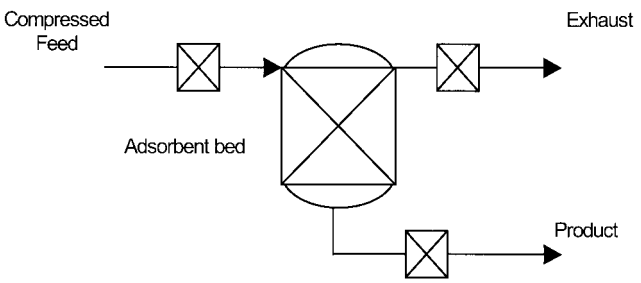

Figure 2. Schematic of pulsed PSA.

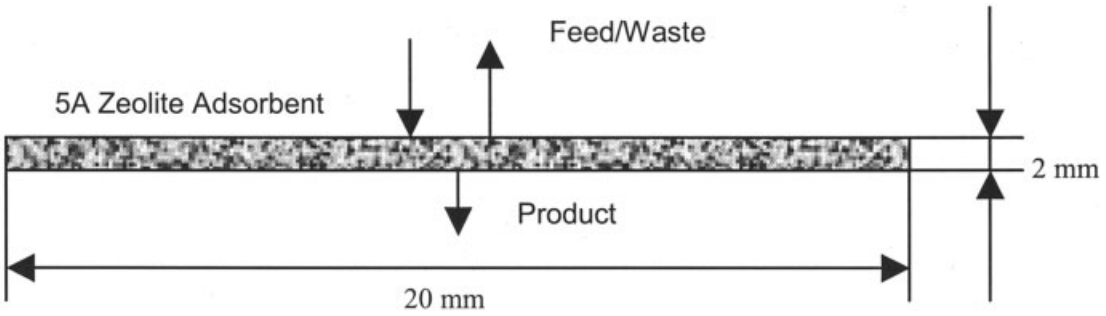

Figure 3. URPSA.

(4) The adsorption rate is described as being either instantaneous or mass-transfer-limited.

(5) There is no pressure gradient in the radial direction. The pressure at the feed entrance is uniformly applied throughout the whole cross-sectional area of the bed.

(6) The ideal gas law is obeyed.

(7) The equilibrium relationships for both oxygen and nitrogen gases are represented by binary Langmuir isotherms.

(8) The boundary conditions at the feed and product ends of the adsorption bed are assumed to be constant during both the pressurization and depressurization parts of the cycle.

(9) The presence of argon, which is adsorbed with the same affinity as oxygen and therefore appears in the product, is ignored.

(10) The molecular weight of the gas is assumed to be constant. This assumption is reasonable, given that the difference in molecular weights of nitrogen and oxygen is small.

(11) The viscosity of air is assumed to be constant. Although the viscosity of a fluid is a function of temperature and pressure, the ranges of temperature and pressure that are investigated here do not have a significant impact on the viscosity.

Based on these assumptions, the following system of equations describes the cyclic operation of the URPSA process.

Overall material balance

$$\frac{\partial P}{\partial t} + \frac{(1-\varepsilon)RT}{\varepsilon M_{air}}(\dot{q}_1 + \dot{q}_2) = -\frac{\partial (PU_x)}{\partial x} \tag{1}$$

Species component balance

$$\frac{\partial p_1}{\partial t} + \frac{(1-\varepsilon)RT}{\varepsilon}\dot{q}_1 = D_{L1}\frac{\partial^2 p_1}{\partial x^2} - \frac{\partial (p_1 U_x)}{\partial x} \tag{2}$$

Mass-transfer-controlled adsorption rate

$$\dot{q}_1 = k_1(q_1^E - q_1) \tag{3}$$

$$\dot{q}_2 = k_2(q_2^E - q_2) \tag{4}$$

or equilibrium-limited adsorption rate

$$\dot{q}_1 = \frac{\partial q_1}{\partial t} = \dot{q}_1^E \tag{5}$$

$$\dot{q}_2 = \frac{\partial q_2}{\partial t} = \dot{q}_2^E \tag{6}$$

Adsorption isotherms

$$q_1^E = \frac{q_{1sat} l_1 p_1}{1 + l_1 p_1 + l_2 p_2} \tag{7}$$

$$q_2^E = \frac{q_{2sat} l_2 p_2}{1 + l_1 p_1 + l_2 p_2} \tag{8}$$

Gas flow velocity

$$U_x = -\frac{b}{\mu}\frac{dP}{dx} \tag{9}$$

Boundary conditions:

(a) Species conservation:

At $x = 0$, the following boundary conditions apply

$$\begin{cases} p_1 = y_1 P_H \rightarrow nt_{cycle} \le t \le nt_{cycle} + t_{pres} \rightarrow \text{pressurization} \\ p_1 = y_1 P_L \rightarrow nt_{cycle} + t_{pres} \le t \le nt_{cycle} + t_{pres} + t_{depr} \\ \quad \rightarrow \text{depressurization} \end{cases} \tag{10}$$

At $x = L$, the following boundary condition applies

$$p_1 = y_1 P_L \tag{11}$$

(b) Total mass balance:

At $x = 0$, the following boundary conditions apply

$$\begin{cases} P = P_H \rightarrow nt_{cycle} \le t \le nt_{cycle} \\ \quad + t_{pres} \rightarrow \text{pressurization} \\ P = P_L \rightarrow nt_{cycle} + t_{pres} \le t \le nt_{cycle} \\ \quad + t_{pres} + t_{depres} \rightarrow \text{depressurization} \end{cases} \tag{12}$$

At $x = L$, the following boundary condition applies

$$P = P_L \tag{13}$$

The initial condition is assumed to be a clean bed with zero adsorption of both nitrogen and oxygen; accommodating a nonzero initial adsorption is trivial to incorporate into the model. The next step in the model development involves introducing dimensionless variables for each of the relevant dependent and independent variables and their relevant derivatives in the describing equations. This is accomplished by employing arbitrary scale and reference factors. Scale factors are introduced to normalize the dimensionless variables to be of order one. Reference factors are introduced to reference the dimensionless dependent or independent variables to zero. The dimensionless variables are then inserted in the describing equations. Then, all terms in the total and species mass-balance equations are divided by the dimensionless coefficient of a term that should be retained (convection term in this case), to ensure that the model has physical significance. This scaling analysis technique has been described in detail by Krantz (1970) and Krantz and Sczechowski (1994). Note that in an earlier article by Kopaygorodsky et al. (2001), the insignificance of mass-transfer limitations inside the monolithic bed has been verified by scaling analysis. Scaling analysis leads to the following minimum parametric representation of the process model for the special case of equilibrium-limited adsorption

$$\frac{\mu L^2}{b(P_H - P_L)t_{pres}}\frac{\partial \hat{P}}{\partial \hat{t}} = -\frac{\partial(\hat{P}\hat{U}_x)}{\partial \hat{x}} - \frac{L^2\mu(1-\varepsilon)RTq_{1sat}l_1}{\varepsilon b(P_H - P_L)t_{pres}}\hat{q}_1^E - \frac{L^2\mu(1-\varepsilon)RTq_{1sat}l_1}{\varepsilon b(P_H - P_L)t_{pres}}\hat{q}_2^E \tag{14}$$

At $\hat{x} = 0$

$$\begin{cases} \hat{P} = 1 & \text{for } 0 \le \hat{t} \le 1 \quad \text{for pressurization} \\ \hat{P} = 0 & \text{for } 1 \le \hat{t} \le 2 \quad \text{for depressurization} \end{cases} \tag{15}$$

At $\hat{x} = 1$

$$\hat{P} = 0 \tag{16}$$

$$\frac{\mu L^2}{t_{pres}b(P_H - P_L)}\frac{\partial \hat{p}_1}{\partial \hat{t}} = \frac{D_{L1}\mu}{b(P_H - P_L)}\frac{\partial^2 \hat{p}_1}{\partial \hat{x}^2} - \frac{\partial(\hat{p}_1\hat{U}_x)}{\partial \hat{x}} - \frac{L^2(1-\varepsilon)RTq_{1sat}l_1\mu}{\varepsilon b(P_H - P_L)t_{pres}}\hat{q}_1^E \tag{17}$$

At $\hat{x} = 0$

$$\begin{cases} \hat{p}_1 = 1 & \text{for } 0 \le \hat{t} \le 1 \quad \text{for pressurization} \\ \hat{p}_1 = 0 & \text{for } 1 \le \hat{t} \le 2 \quad \text{for depressurization} \end{cases} \tag{18}$$

At $\hat{x} = 1$

$$\hat{p}_1 = 0 \tag{19}$$

Table 1. Parameter Values Used in the Simulation of URPSA

System Parameters	Conventional PSA	Ultra-Rapid PSA
L (m)	1.0	2.0×10^{-3}
P_L (Pa)	1×10^5	1×10^5
P_H (Pa)	1.3×10^5	1.5×10^5
D_{L2} (m^2/s)	10^{-10}	10^{-10}
b (m^2)	6.76×10^{-10}	2.71×10^{-15}
k_i (s^{-1})	0.006	1.5×10^3
$q_{1sat} \times l_1$ (mol/m^3 · Pa)	0.0014	0.0014
$q_{2sat} \times l_2$ (mol/m^3 · Pa)	0.0004	0.0004
T (K)	293	293
ε	0.35	0.35
t_{pres}	50	1
t_{depres}	50	2
D_{L1} (m^2/s)	10^{-5}	10^{-6}
$R_{p/c}$ (m)	0.5×10^{-3}	1×10^{-6}

$$\hat{q}_1^E = \frac{[\hat{p}_1 + P_L/(P_H - P_L)]}{1 + l_1(P_H - P_L)[\hat{p}_1 + P_L/(P_H - P_L)]} \tag{20}$$

$$\hat{q}_2^E = \frac{[\hat{p}_2 + P_L/(P_H - P_L)]}{1 + l_2(P_H - P_L)[\hat{p}_2 + P_L/(P_H - P_L)]} \tag{21}$$

$$\hat{q}_1^E = \{1 + l_1(P_H - P_L)[\hat{p}_1 + P_L/(P_H - P_L)]\}^{-2}\frac{d\hat{p}_1}{d\hat{t}} \tag{22}$$

$$\hat{q}_2^E = \{1 + l_2(P_H - P_L)[\hat{p}_2 + P_L/(P_H - P_L)]\}^{-2}\frac{d\hat{p}_2}{d\hat{t}} \tag{23}$$

Process Parameter Values

The equilibrium and kinetic parameters for URPSA are summarized in Table 1, along with bed dimensions, particle size, and cycle times. For the purpose of comparison, parameter values typical for conventional PSA are also shown in Table 1, where L is the thickness of the adsorption bed; P_L is the pressure at the product side of the bed; P_H is the feed pressure; D_{L2} is the intracrystalline diffusion coefficient, obtained from Ruthven and Xu (1993); k_i is the mass-transfer coefficient for species i; $b = \varepsilon^3(2R_p)^2/150(1-\varepsilon)^2$ is the Darcy's law constant; t_{pres} and t_{depres} are the pressurization and depressurization times, respectively; $R_{p/c}$ is the radius of the zeolite crystal; and $q_{1sat} \times l_1$ and $q_{2sat} \times l_2$ are equilibrium adsorbent properties for N_2 and O_2 gases, respectively, obtained from the publication by Liow and Keeney (1990). D_{L1} is the axial dispersion coefficient determined by the following approximation

$$D_{L1} = \gamma_1 D_m + \gamma_2 ud \tag{24}$$

where γ_1 and γ_2 are constants having values of approximately 0.7 and 0.5, respectively; d is the diameter of the zeolite crystal; u is the velocity through the porous medium; and D_m is the molecular diffusivity calculated by the Chapman–Enskog equation [for example, Bird et al. (1960); Brodkey and Hershey (1988); Ruthven (1984)]:

$$D_m = \frac{0.00158T^{3/2}\left(\frac{1}{M_1} + \frac{1}{M_2}\right)^{1/2}}{P\sigma_{12}^2\Omega} \quad (25)$$

where M_1 and M_2 are the molecular weights of nitrogen and oxygen respectively, P is the total pressure in atmospheres, $\sigma_{12} = (\sigma_1 + \sigma_2)/2$ is the collision diameter from the Lennard–Jones potential, $\Omega = \sqrt{\varepsilon_1\varepsilon_2}/k_BT$ where ε_i is the force constant of species i, and k_B is Boltzmann's constant.

The mass-transfer coefficient k_i characterizes the mass-transfer limitation inside the adsorbent particles in the context of conventional PSA and inside the zeolite crystals in the context of URPSA. If the adsorption rate is described by Eqs. 3 and 4, the mass-transfer coefficient has to be estimated using the following expression, which is valid for both conventional PSA and URPSA, according to Alpay and Kenney (1993)

$$k_i = 15\,\frac{D_{L2}}{R_{p/c}^2} \quad (26)$$

These values of the process parameters permit determining the coefficients in front of various terms in the describing equations. The resulting values of the dimensionless groups in these equations then permit assessing when certain approximations, frequently made in modeling the conventional PSA process, apply to the URPSA process. This is done in the next section.

Justifying Approximations

The six dimensionless groups emanating from Eqs. 14−25 and the group characterizing the relative importance of intraparticle mass transfer are summarized below

$$N_1 \equiv \frac{\mu L^2}{t_{pres}b(P_H - P_L)} \quad (27)$$

$$N_2 \equiv \frac{RT(1-\varepsilon)q_{1sat}l_1\mu L^2}{t_{pres}\varepsilon b(P_H - P_L)} \quad (28)$$

$$N_3 \equiv \frac{RT(1-\varepsilon)q_{2sat}l_2\mu L^2}{t_{pres}\varepsilon b(P_H - P_L)} \quad (29)$$

$$N_4 \equiv l_1(P_H - P_L) \quad (30)$$

$$N_5 \equiv l_2(P_H - P_L) \quad (31)$$

$$N_6 \equiv \frac{D_{L1}\mu}{b(P_H - P_L)} \quad (32)$$

$$N_7 = \frac{1}{k_i t_1} \quad (33)$$

The group N_1 permits assessing the relative importance of the unsteady-state term in the overall and component mass balances. The group N_2 permits assessing the importance of mass loss attributed to adsorption in the nitrogen mass balance. Groups N_2 and N_3 permit assessing the importance of adsorption of nitrogen and oxygen, respectively, in the overall mass balance. Groups N_4 and N_5 permit determining when the Langmuir adsorption isotherms reduce to linear relationships, that is, Henry's law type approximations. The group N_6 is a measure of the importance of axial dispersion in the bed. The group N_7, derived by Kopaygorodsky et al. (2001), is a measure of the significance of the mass-transfer limitation inside the adsorbent particles. By inserting the values of the process parameters (Table 1) into Eqs. 27–33, the groups N_1, N_2, N_3, N_4, N_5, N_6, and N_7 can be calculated to assess the relative importance of the various terms in the describing equations for both the conventional PSA and URPSA processes. Table 2 summarizes the values of these seven dimensionless groups.

Table 2. Characteristic Dimensionless Groups for Conventional PSA and URPSA

Dimensionless Group	Conventional PSA	Ultra-Rapid PSA
N_1	0.011	0.54
N_2	0.11	3.4
N_3	0.03	0.9
N_4	0.015	0.025
N_5	0.0054	0.009
N_6	9.0×10^{-6}	0.136
N_7	3.3	0.0007

One sees that these two processes are markedly different. The magnitude of N_1 indicates that the conventional PSA process is quasi-steady state; that is, one can safely neglect the unsteady-state term in the overall mass balance when determining the pressure distribution in conventional packed beds. However, this assumption cannot be made for URPSA. The magnitude of N_2 indicates that in the conventional PSA process one can ignore the rate of nitrogen adsorption when solving the nitrogen mass balance. It is important to note that nitrogen is still getting adsorbed in the conventional columns; it is just that the adsorption rate is not sufficient to significantly influence the partial pressure of nitrogen in the bed. However, the nitrogen adsorption term is important in the species conservation equation for the URPSA process. The magnitudes of N_2 and N_3 determine the importance of the nitrogen and oxygen rates of adsorption in the overall mass balance. One sees that in the context of conventional PSA, the nitrogen and oxygen adsorption rates are not important in determining the total pressure profiles in the bed. However, in the context of URPSA, these terms have to be retained to accurately determine the total pressure distribution in the bed. The magnitudes of the groups N_4 and N_5 indicate that the adsorption equilibrium can be described by a simple linear relationship for both the conventional PSA as well as for URPSA processes. The magnitude of N_6 indicates that axial dispersion is not important in the context of conventional PSA. However, this term is important for URPSA. The magnitude of N_7 shows the significance of the mass-transfer limitation inside the adsorbent particles for conventional packed columns and justifies the assumption of equilibrium adsorption for the novel URPSA process reported in this study.

The magnitude of the dimensionless groups in front of the various terms in the describing equations indicates that none of the usual simplifying approximations made in the species conservation equation and total mass balance can be justified for

the URPSA process. The only approximation justified for the URPSA process is that the adsorption isotherm can be modeled by a linear Henry's law type approximation. Thus, based on the value of dimensionless group N_4, Eqs. 22 and 23 can be simplified as follows

$$\hat{q}_1^E = \frac{d\hat{p}_1}{d\hat{t}} \tag{34}$$

$$\hat{q}_2^E = \frac{d\hat{p}_2}{d\hat{t}} \tag{35}$$

Inserting Eqs. 21 and 34 into Eq. 17 and combining the adsorption with the unsteady-state term in the species mass-balance equation results in the following

$$\left[\frac{\mu L^2}{t_{pres} b(P_H - P_L)} + \frac{L^2 \mu (1-\varepsilon) RT q_{1sat} l_1}{\varepsilon b (P_H - P_L) t_{pres}}\right] \frac{\partial \hat{p}_1}{\partial \hat{t}} = \frac{D_{L1}\mu}{b(P_H - P_L)} \frac{\partial^2 \hat{p}_1}{\partial \hat{x}^2} + \left(\frac{\partial \hat{p}_1}{\partial \hat{x}}\right)\left(\frac{\partial \hat{P}}{\partial \hat{x}}\right) + \hat{p}_1 \frac{\partial^2 P}{\partial x^2} \tag{36}$$

Inserting Eqs. 21, 34, and 35 into Eq. 14 then results in the following form for the total mass-balance equation

$$\frac{\mu L^2}{t_{pres} b(P_H - P_L)} \frac{\partial \hat{P}}{\partial \hat{t}} = -\left[-\left(\frac{\partial \hat{P}}{\partial \hat{x}}\right)^2 - \hat{P} \frac{\partial^2 \hat{P}}{\partial \hat{x}^2}\right] - \left[\frac{RT(1-\varepsilon) q_{1sat} l \mu L^2}{t_{pres} \varepsilon b (P_H - P_L)} \frac{\partial \hat{p}_1}{\partial \hat{t}} + \frac{RT(1-\varepsilon) q_{2sat} l \mu L^2}{t_{pres} \varepsilon b (P_H - P_L)} \frac{\partial \hat{p}_2}{\partial \hat{t}}\right] \tag{37}$$

Solution Methodology

Visual Simulation version 5.0 (VisSim™) of Visual Solutions, Inc. (487 Groton Road, Westford, MA 01886) is a comprehensive software for solving real-world engineering problems and simulating the dynamics of linear and nonlinear systems. There are several advantages to using Visual Simulation software when trying to generate a solution to the URPSA process model. First, VisSim runs on PCs and compatibles. Because VisSim operates on Windows, it allows the user to construct block-diagram models using familiar point-and-click commands and requires no knowledge of UNIX or any programming language. Second, VisSim contains numerous features that are necessary to generate a solution to the mathematical model of the process under investigation in this research. For example, any simulation on VisSim can be run in real or dimensionless time. Because the model constructed for the URPSA process is scaled and expressed in dimensionless form, this feature is very important. In addition, VisSim can exchange information with other Windows applications. This capability was used to report the results of the simulation. One of the most important features for this work is the ability of VisSim to integrate stiff problems. Visual Simulation offers seven integration methods. One of these integration methods is the Backward Euler (Stiff). This integrator takes very small steps in time and handles steep time derivatives very well. The aforementioned advantages and the accessibility of this software package contributed to a decision to use it in this research.

Table 3. Process Parameters and Dimensionless Groups for the Experiments of Pritchard and Simpson (1986)

System Parameters	Rapid PSA
b (m^2)	6.76×10^{-11}
l (m^2/N)	5.15×10^{-7}
k_i	0.05
L (m)	0.23
P_H (Pa)	1.68×10^5
P_L (Pa)	1×10^5
ε	0.35
t_1 (s)	1.5
t_2 (s)	4
D_{L1} (m^2/s)	10^{-5}
D_{L2} (m^2/s)	10^{-10}
R_p (m)	1.77×10^{-4}
N_1	0.14
N_2	0.9
N_3	0.26
N_4	0.037
N_5	0.012
N_6	4.0×10^{-5}
N_7	13

Partial differential equations can be solved on VisSim by the finite-difference method. The finite-difference method is a transformation that reduces two continuous independent variables (x and t) to a discrete variable x and a continuous variable t. Replacing the continuous variable x with the number of discrete axial points in Eqs. 36 and 37 allows converting these partial differential equations into ordinary differential equations. This means that the solution will be in terms of discrete space and continuous time. Because VisSim is capable of exchanging information with other Windows applications, the output in terms of continuous time and discrete space can be converted to continuous space at discrete times.

Model Consistency Study

Before attempting to use the model developed here to assess the potential for URPSA, it is essential to establish the validity of this new model. Unfortunately there are no experimental data for URPSA because this is an entirely new concept. However, there are data available for the performance of Rapid Pressure Swing Adsorption (RPSA), those of Pritchard and Simpson (1986), that can be used to assess the consistency of the model developed here. Pritchard and Simpson's experimental apparatus consisted of interchangeable columns, 38 mm in diameter and having different lengths, a surge tank with a product takeoff regulating valve and flow meter, and a series of associated valves. The operating cycle of their apparatus consisted of five steps: pressurization (0.1 s), feed (1 s), delay (0.5 s), depressurization (0.1 s), and exhaust (4 s). In their experiment, a chromatographic grade of 5A zeolite was used as the adsorbent, with 60–80 mesh (250–177 μm) particle size. Their study was directed toward investigating the potential of the RPSA process to provide high (85%) and low (30%) enriched air. Table 3 lists the values of the process parameters used in Pritchard and Simpson's experiments for the low enrichment RPSA process along with the values of the seven dimensionless groups characterizing PSA that were identified in the present study. The process parameters listed in Table 3 were used as input parameters in the model developed here. The resulting predicted oxygen purity of 33% is higher than the experimental

Table 4. Comparison of Predicted Performance for Conventional PSA and URPSA

Process	Oxygen Purity (%)	Product Recovery (%)	Bed-Size Factor
Conventional PSA	92	19	0.2
Ultra-Rapid PSA	85	56	7.1×10^{-3}

value of 28%. The reason for this disparity is because the model developed here ignores any mass-transfer limitations and assumes an equilibrium adsorption rate. Although this is justified for URPSA, it is a tenuous assumption for RPSA because of the fact that the dimensionless group N_7, which is a measure of the relative importance of mass-transfer limited adsorption, is not small enough to justify neglecting this term. Indeed, ignoring this term for RPSA will result in overestimating the oxygen purity. On the basis of this agreement between the model predictions and RPSA performance data, we can proceed with confidence to use this model to assess the potential of URPSA.

Results and Discussion

The following model performance characteristics were reported: oxygen purity, product recovery, and bed-size factor (BSF). Product recovery and the bed-size factor are defined as follows

$$R_{O_2} = \frac{y_{O_2}|_{product} Q_{product}}{y_{O_2}|_{feed} Q_{feed}} \times 100\% \tag{38}$$

where $y_{O_2}|_{feed}$ and $y_{O_2}|_{product}$ are the oxygen mole fractions in the feed and product, respectively, and Q_{feed} and $Q_{product}$ are the feed and product flow rates, respectively

$$\text{BSF} = \frac{m_{ad}}{m_{O_2}} \tag{39}$$

where m_{ad} is the mass of adsorbent in tons and m_{O_2} is the mass of produced oxygen in tons per day. For the sake of comparison, oxygen purity, recovery, and the bed-size factor determined by the model for URPSA process and the same performance characteristics, determined by Farooq et al. (1989) for the conventional PSA process, are reported in Table 4. For this comparison, typical parameters were used to model the PSA process and currently feasible parameters were used for the URPSA process. However, no attempt was made to optimize either the PSA or URPSA process. Table 4 shows that the two processes are markedly different. There is a significant difference in the bed-size factor and product recovery. The high product recovery and smaller value of the bed-size factor obtained for URPSA process are a result of the increased efficiency of separation per unit mass of monolithic adsorbent material.

It is convenient to study the effects of the adsorbate/adsorbent properties, monolithic adsorbent bed characteristics, and operating conditions on the URPSA process by casting the results in dimensionless form. This permits representing the model results by a minimum parametric representation and thereby generalizing the predictions. However, the six dimensionless groups (N_7 drops out of the analysis if mass-transfer limitations to adsorption can be ignored) that were obtained by scaling analysis, although convenient for assessing the applicability of the various simplifying assumptions, are not optimal for presenting the model results. The latter are presented optimally in dimensionless form by isolating the parameters that characterize the adsorbent/adsorbate properties and monolith adsorbent bed characteristics into dimensionless groups that do not contain any of the operating conditions. Moreover, if possible, it is desirable to isolate each major operating condition into one dimensionless group. A systematic method for doing this is described by Krantz (2000). Application of this systematic method yields the following set of independent dimensionless groups that are optimal for representing the predictions of the URPSA model developed here

$$N'_6 = \frac{N_2}{N_3} = \frac{q_{1sat} l_1}{q_{2sat} l_2} \tag{40}$$

$$N'_7 = N_4 N_5 = \frac{D_{L1} \mu l}{b} \tag{41}$$

$$N_8 = \frac{N_1}{N_3} = \frac{\varepsilon}{RT(1-\varepsilon) q_{2sat} l_2} \tag{42}$$

$$N_9 = N_1 N_4 = \frac{\mu L^2 l}{t_{pres} b} \tag{43}$$

$$N_4 \equiv l_1 (P_H - P_L) \tag{44}$$

$$N_{10} = \frac{N_7}{N_9} = \frac{t_{pres} D_{L1}}{L^2} \tag{45}$$

$$N'_{10} = \frac{N_7}{N_9} = \frac{t_{depres} D_{L1}}{L^2} \tag{46}$$

Note that N_6, N_7, and N_8 depend only on the adsorbate/adsorbent bed properties and monolith adsorbent bed characteristics and hence are constant once the air/adsorbent system is specified. The dimensionless group N_{10} isolates the bed length and pressurization time, whereas N'_{10} isolates the adsorbent bed length and depressurization time. The group N_4 isolates the pressure swing.

The dimensional analysis is performed in this section under the assumption of constant physical and equilibrium properties of the adsorbent material. That is, the values of dimensionless groups N_6, N_7, and N_8 are kept constant. The effect of feed pressure on product recovery and product purity at different pressurization times is illustrated in Figures 4 and 5. According to the results of the model, an increase in the dimensionless group N_4 leads to an increase in the product recovery. This can be explained by the fact the higher values of group N_4 results in larger pressure gradients across the bed and, thus, higher throughputs. An increase in the value of dimensionless group N_{10} results in lower product recoveries. This can be explained by the decreased throughput caused by the higher gas loading on the surface of the adsorbent material at longer pressurization times. An increase in the dimensionless group N_4 results in

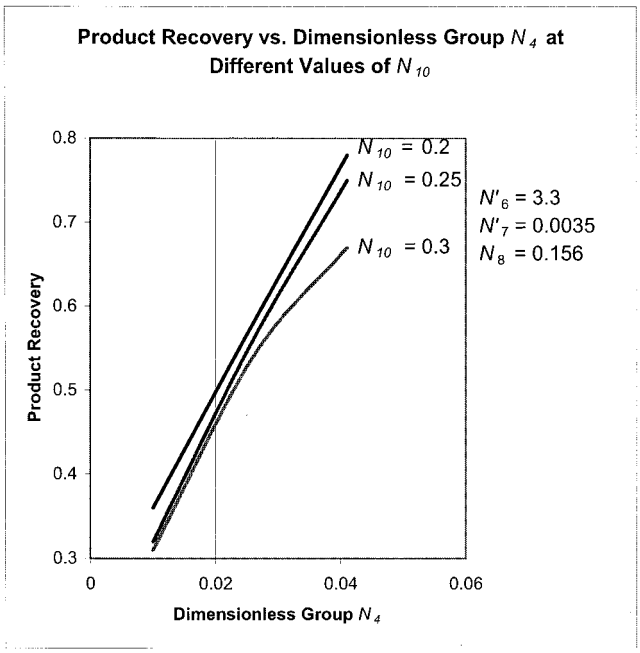

Figure 4. Product recovery vs. N_4 at different values of N_{10}.

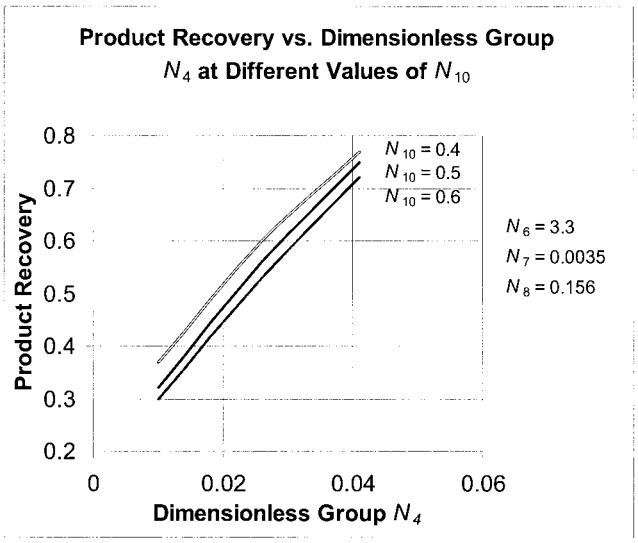

Figure 6. Product recovery vs. N_4 at different values of N_{10} and N'_{10}.

smaller values of the product purity, which can be explained by decreased contact times. Product purity is also inversely related to the dimensionless group N_{10}. Longer pressurization times limit the adsorbent capacity on the bed. Note that an increase in the dimensionless group N_{10} can also be attributed to a decrease in the bed length.

The same dimensional analysis has been performed here to determine the impact of dimensionless groups N_4 and N'_{10} on the predicted performance characteristics while keeping the other groups constant. Because groups N_4 and N'_{10} are functions of feed pressure and depressurization time, respectively, the impact of these important process parameters on product recovery and product purity can be determined. Figures 6 and 7 shows the impact of dimensionless groups N_4 and N'_{10} on product recovery and product purity, while keeping groups N_6, N_7, and N_8 constant. The increase in the value of the dimensionless group N'_{10} has a negative impact on the product recovery because at longer depressurization times, the adsorbent is regenerated to a greater extent. More gas molecules are adsorbed on the surface during pressurization, which causes smaller throughput. However, at longer depressurization times (larger value of dimensionless group N'_{10}), the product purity is improved. This is also attributed to the greater regeneration of the adsorbent material.

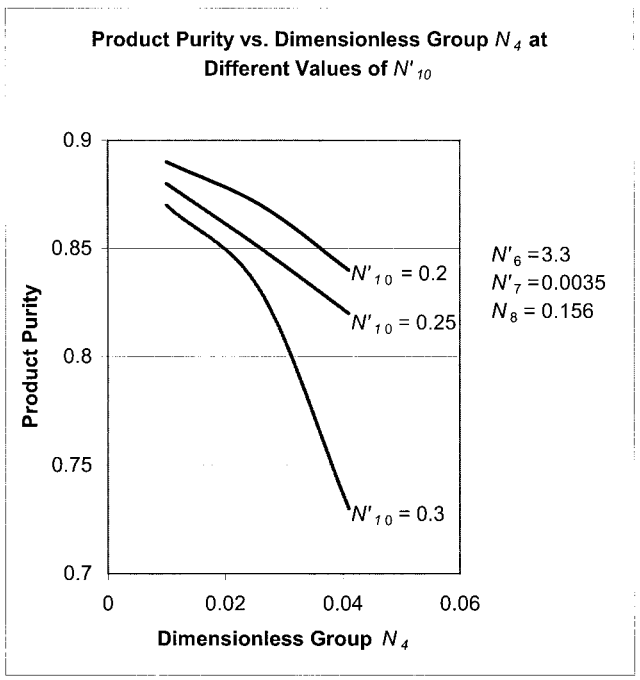

Figure 5. Product purity vs. N_4 at different values of N'_{10}.

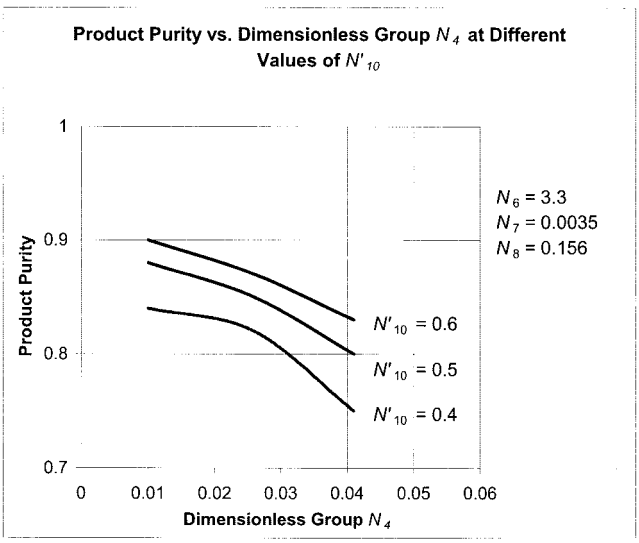

Figure 7. Product purity vs. N_4 at different values of N_{10} and N'_{10}.

Conclusions

Scaling analysis has been used to achieve the minimum parametric representation for the PSA process. The resulting minimum parametric representation permits assessing the validity of simplifying assumptions that have been invoked to describe PSA processes. The various dimensionless groups emanating from the scaling analysis have been evaluated for the special case of using both conventional PSA and URPSA to produce oxygen from air using a 5A zeolite adsorbent. The scaling analysis indicates that the novel URPSA process proposed here differs markedly from conventional PSA for the production of oxygen from air. In particular, whereas conventional PSA can usually be assumed to operate under quasi-steady-state conditions, this is never true for URPSA because of the rapid pressurization and depressurization times. Moreover, although the effect of nitrogen and oxygen adsorption has a negligible effect on the total pressure for conventional PSA, it has a significant effect for URPSA because of the markedly increased adsorption capacity of the monolithic adsorbents used in URPSA. Finally, although the rate of adsorption in conventional PSA is usually limited by intraparticle mass transfer, it is essentially dictated by equilibrium adsorption for the small 5A zeolite crystal monolith adsorbent used in URPSA.

The most important conclusion emanating from this study is that URPSA is capable of producing an oxygen purity of 85% with a product recovery of 56% from an air feed using a pressure swing of 50–80 kPa, a pressurization time of 0.8–1.2 s, a depressurization time of 1.6–2.4 s, with a 5A zeolite monolith adsorbent bed having a thickness of 2 mm and a diameter of 20 mm. The predicted product recovery is significantly higher than that achieved by conventional PSA. It is noteworthy that URPSA can achieve comparable oxygen purity with a bed-size factor more than two orders of magnitude smaller than typical values for conventional PSA. This is of particular importance to the economics of URPSA, given that the bed-size factor is the ratio of the mass of adsorbent required per unit mass of oxygen produced per day.

The results of this study suggest that URPSA is a viable process that should offer significant advantages over conventional PSA as well as other separation technologies for producing oxygen from air. The potential of URPSA for other gas separations needs to be explored as well. This study provides strong support to research efforts to develop the monolith adsorbents required in the URPSA process.

Acknowledgment

The authors thank the National Science Foundation for providing funding for this research (NSF/CTS-0100087).

Notation

A = area of the adsorption bed, m^2
b = characteristic of a particular adsorbent, m^2
BSF = bed-size factor defined by Eq. 39
d = diameter of zeolite crystals, m
D_{L1} = axial dispersion coefficient, m^2/s
D_{L2} = intraparticle diffusivity, m^2/s
D_{2L} = diffusivity within the micropores of a zeolite crystal, m^2/s
D_m = molecular diffusivity, m^2/s
k_B = Boltzmann's constant, J/mol·K
k_i = intraparticle mass transfer coefficient for species i, s^{-1}
L = thickness of adsorbent bed, m
l_1 = equilibrium van't Hoff constant for N_2, m^2/N
l_2 = equilibrium van't Hoff constant for O_2, m^2/N
M_{air} = molecular weight of air, kg/mol
M_1 = molecular weight of N_2
M_2 = molecular weight of O_2
m_{ad} = mass of adsorbent, tons
m_{O_2} = mass of produced oxygen, tons
n = number of PSA cycles
P = total pressure in the bed, Pa
P_H = total feed pressure, Pa
P_L = total pressure at the product side of adsorbent bed, Pa
p_1 = partial pressure of nitrogen, Pa
p_{1H} = partial pressure of nitrogen at the feed surface of adsorption bed, Pa
p_{1L} = partial pressure of nitrogen at the product end of adsorption bed, Pa
Q_{feed} = feed flow rate, mol/s
$Q_{product}$ = product flow rate, mol/s
$\dot{q}$ = amount of property generated or depleted, $mol/m^3 \cdot s$
$\dot{q}_1$ = rate of nitrogen adsorption per unit volume of adsorbent bed, $mol/m^3 \cdot s$
$\dot{q}_2$ = rate of oxygen adsorption per unit volume of adsorbent bed, $mol/m^3 \cdot s$
$\dot{q}_1^E$ = equilibrium nitrogen adsorption rate, $mol/m^3 \cdot s$
q_1^E = equilibrium adsorbed phase nitrogen concentration, mol/m^3
q_1 = actual adsorbed phase nitrogen concentration, mol/m^3
q_{1sat} = saturated value of adsorbed phase nitrogen concentration, mol/m^3
q_2^E = equilibrium adsorbed phase oxygen concentration, mol/m^3
q_{2sat} = saturated value of adsorbed phase oxygen concentration, mol/m^3
R = gas constant, $Pa \cdot m^3/mol \cdot K$
R_{O_2} = oxygen product recovery defined by Eq. 38
$R_{p/c}$ = radius of a particle or a crystal, m
T = absolute temperature, K
t = time, s
t_{cycle} = total cycle time, s
t_{pres} = pressurization time, s
t_{depres} = depressurization time, s
t_1 = time of pressurization step in the cycle, s
t_2 = time of depressurization step in the cycle, s
u = velocity through the porous medium, m/s
U_x = velocity of mass in the axial direction, m/s
x = axial direction, m
y_1 = mole fraction of nitrogen
y_2 = mole fraction of oxygen
$y_{O_2 \mid feed}$ = oxygen mole fraction in the feed
$y_{O_2 \mid product}$ = oxygen mole fraction in the product
ε = bed voidage
ε_i = force constant of species i, J/mol
γ_1, γ_2 = constants in Eq. 24 having values of 0.7 and 0.5, respectively
μ = shear viscosity of air, Pa·s
σ_i = molecular collision diameter from the Lennard–Jones potential, m

Definitions of dimensionless variables

$$\hat{x} \equiv \frac{x}{x_s}$$

$$\hat{t} \equiv \frac{t}{t_s}$$

$$\hat{U} \equiv \frac{U}{U_s}$$

$$\frac{\partial U}{\partial x} \equiv \frac{1}{U_{xs}} \frac{\partial U}{\partial x}$$

$$\hat{P} \equiv \frac{P - P_r}{P_s}$$

$$\hat{\dot{q}} \equiv \frac{\dot{q}}{\dot{q}_s}$$

$$\hat{q} \equiv \frac{q_P^E}{q_s}$$

where the subscript s denotes a scale factor and the subscript r denotes a reference factor. Scale factors are introduced to normalize the dimensionless variables to be of order one. Reference factors are introduced to reference the dimensionless dependent or independent variables to zero.

Definitions of dimensionless groups

- N_1 permits assessing the relative importance of the unsteady-state term in the overall and component mass balances.
- N_2 permits assessing the importance of mass loss attributed to adsorption in the nitrogen mass balance.
- N_2 and N_3 permit assessing the importance of adsorption of nitrogen and oxygen, respectively, in the overall mass balance.
- N_4 and N_5 permit determining when the Langmuir adsorption isotherms reduce to linear relationships, that is, Henry's law type approximations.
- N_6 is a measure of the importance of axial dispersion in the bed.
- N_7 is a measure of the significance of the mass-transfer limitation inside the adsorbent particles.
- See text for definitions of additional dimensionless groups N'_6, N'_7, N_8, N_9, N_{10}, and N'_{10}, according to Eqs. 40–46.

Literature Cited

Alpay, E., C. N. Kenney, and D. M. Scott, "Simulation of Rapid Pressure Swing Adsorption and Reaction Processes," *Chem. Eng. Sci.*, **48**, 3173 (1993).

Alpay, E., C. N. Kenney, and D. M. Scott, "Adsorbent Particle Size Effect in the Separation of Air by Rapid Pressure Swing Adsorption," *Chem. Eng. Sci.*, **49**, 3059 (1994).

Bird, R. B., W. E. Stewart, and E. N. Lightfoot, *Transport Phenomena*, Wiley, New York (1960).

Brodkey, R. S., and H. C. Hershey, *Transport Phenomena*, McGraw-Hill Chemical Engineering Series, New York (1988).

Carter, J. W., "Numerical Method for Prediction of Adiabatic Adsorption in Fixed Beds," *Trans. Inst. Chem. Eng.*, **44**, T253 (1966).

Ergun, S., "Fluid Flow Through Packed Columns," *Chem. Eng. Prog.*, **48**, 89 (1952).

Farooq, S., D. M. Ruthven, and H. A. Boniface, "Numerical Simulation of Pressure Swing Adsorption Oxygen Unit," *Chem. Eng. Sci.*, **44**, 2809 (1989).

Glueckauf, E., and J. J. Coates, "Theory of Chromatography: IV. The Influence of Incomplete Equilibrium of the Front Boundary of Chromatograms and on the Effectiveness of Separation," *J. Chem. Soc.*, 1315 (1947).

Hart, J., and W. J. Thomas, "Gas Separation by Pulsed Pressure Swing Adsorption," *Gas Sep. Purif.*, **5**, 125 (1991).

Hassan, M. M., and D. M. Ruthven, "Air Separation by Pressure Swing Adsorption on Carbon Molecular Sieve," *Chem. Eng. Sci.*, **41**, 1333 (1986).

Jones, R. L., and G. E. Keller, "Pressure Swing Parametric Pumping—A New Adsorption Process," *Sep. Process Technol.*, **2**, 17 (1981).

Jones, R. L., and G. E. Keller, "Rapid Pressure Swing Adsorption Process with High Enrichment Factor," U.S. Patent 4,194,892, assigned to Union Carbide Corporation (March 25, 1980).

Karger, J., and D. M. Ruthven, *Diffusion in Zeolites*, Wiley, New York (1992).

Krantz, W. B., "Scaling Initial and Boundary Value Problems as a Teaching Tool for a Course of Transport Phenomena," *Chem. Eng. Ed.*, **4**, 145 (1970).

Krantz, W. B., "An Alternate Method for Teaching and Implementing Dimensional Analysis," *Chem. Eng. Ed.*, **34**, 216 (2000).

Krantz, W. B., and J. G. Sczechowski, "Scaling Initial and Boundary Value Problems: A Tool in Chemical Engineering and Practice," *Chem. Eng. Ed.*, **28**, 236 (1994).

Kopaygorodsky, E. M., W. B. Krantz, and V. V. Guliants, "Scaling Analysis—A Valuable Technique in Engineering Teaching and Practice," *Proc. 2001 Am. Soc.r Eng. Ed. Annu. Conf. Exposition*, Section 3513 (2001).

Liow, J.-L., and C. N. Kenney, "The Backfill Cycle of the Pressure Swing Adsorption Process," *AlChE J.*, **36**, 53 (1990).

Mendes Adelio, M. M., and M. V. Costa, "Analysis of Nonisobaric Steps in Nonlinear Bicomponent Pressure Swing Adsorption Systems. Application for Air Separation," American Chemical Society, Washington, DC, Published on Web (1999).

Pritchard, C. L., and G. K. Simpson, "Design of an Oxygen Concentrator Using the Rapid Pressure-Swing Adsorption Principle," *Chem. Eng. Res. Des.*, **64**, 467 (1986).

Raghavan, N. S., M. M. Hassan, and D. M. Ruthven, "Numerical Simulation of a PSA System. Part I: Isothermal Trace Component System with Linear Equilibrium and Finite Mass Transfer Resistance," *AIChE J.*, **31**, 385 (1985).

Rota R., and P. C. Wankat, "Intensification of Pressure Swing Adsorption Processes," *AIChE J.*, **36**, 1299 (1990).

Ruthven, D. M., *Principles of Adsorption and Adsorption Processes*, Wiley, New York (1984).

Ruthven, D. M., S. Farooq, and K. S. Knaebel, *Pressure Swing Adsorption*, VCH Publishers, New York (1994).

Ruthven, D. M., and Z. Xu, "Diffusion of Oxygen and Nitrogen in 5A Zeolite Crystals and Commercial 5A Pellets," *Chem. Eng. Sci.*, **48**, 3307 (1993).

Shendalman, L. H., and J. E. Mitchell, "Heatless Adsorption in the Model System CO_2 in He, I.," *Chem. Eng. Sci.*, **27**, 1449 (1972).

Shin, H.-S., and K. S. Knaebel, "Pressure Swing Adsorption: A Theoretical Study of Diffusion-Induced Separations," *AIChE J.*, **33**, 654 (1987).

Singh, K., and J. Jones, "Numerical Simulation of Air Separation by Piston-Driven Pressure Swing Adsorption," *Chem. Eng. Sci.*, **52**, 3133 (1987).

Teague, K. G., and T. F. Edgar, "Predictive Dynamic Model of a Small Pressure Swing Adsorption Air Separation Unit," *Ind. Eng. Chem. Res.*, **38**, 3761 (1999).

Turnock, P. H., and R. H. Kadlec, "Separation of Nitrogen and Methane via Periodic Adsorption," *AIChE J.*, **17**, 335 (1971).

Manuscript received Oct. 4, 2002, and revision received July 11, 2003.